Magnetic Resonance in Medicine 43:151–154 (2000)

Automatic Field Map Generation and Off-Resonance Correction for Projection Reconstruction Imaging

Krishna S. Nayak* and Dwight G. Nishimura

A new projection reconstruction technique utilizes the oversampling of low spatial frequencies to estimate and correct for off-resonance effects. Interleaved spokes are acquired at one of two different echo times. From separated early-TE and late-TE raw data, two one-quarter resolution images are reconstructed and a one-quarter resolution field map is computed. Multifrequency reconstruction with all the data is then used to simultaneously correct for off-resonance and compensate for the difference in echo times. Resulting images obtained on phantoms and in vivo demonstrate significantly reduced off-resonance artifact without the acquisition of a separate field map. Magn Reson Med 43:151–154, 2000. © **2000 Wiley-Liss, Inc.**

Key words: projection reconstruction; off-resonance; pulse sequences; reconstruction

Projection reconstruction (PR) is a popular MR imaging technique. PR is gaining increasing popularity because of its ability to achieve short echo times and to produce images with minimal motion or flow artifacts. Short echo times are particularly important in the imaging of short T_2 species (1) and in rapid imaging (2). Reduced motion artifacts (3) are important again for dynamic imaging, and particularly for angiography (4) and functional MRI (5).

Inherent in PR imaging is the oversampling near the *k*-space origin. This is considered to be a strong advantage because it is well known that the low spatial frequencies contain most of the energy in images. This oversampling can however be exploited to improve imaging in other ways. For example, image field of view (FOV) is often calculated based on an inner area of *k*-space, tolerating spoke artifacts from insufficiently sampling the outer regions (6–9).

One drawback of PR is that off-resonant spins cause blurring. The most common way to compensate for this blurring involves acquiring a field map with an additional scan and using a frequency-sensitive reconstruction to compensate for off-resonance (10,11).

We present a technique that corrects for off-resonance without a separate field-map acquisition. This technique incorporates a field map acquisition within PR imaging by interleaving spokes with two different echo times (TEs). The acquired data is then used both to generate a low-resolution field map, and to reconstruct the final image with off-resonance correction. Results from phantom studies and in vivo studies are presented.

THEORY

In MR imaging, the Fourier relationship between image domain and *k*-space, yields the following signal equation

$$S(t) = \int_{x,y} M(x, y)e^{-2\pi i(k_x(t)x + k_y(t)y)}\, dx\, dy \qquad [1]$$

where $M(x, y)$ is the imaging slice and $k_x(t)$ and $k_y(t)$ are the *k*-space trajectories determined by the linear gradients fields; that is, $k_x(t) = \gamma/2\pi \int_0^t G_x(\tau)\, d\tau$ and $k_y(t) = \gamma/2\pi \int_0^t G_y(\tau)\, d\tau$. In the presence of field inhomogeneity or off-resonance the signal equation translates into the relationship shown in Eq. [2].

$$S(t) = \int_{x,y} [M(x, y)e^{-2\pi i\Delta f(x,y)t}]e^{-2\pi i(k_x(t)x + k_y(t)y)}\, dx\, dy \qquad [2]$$

where $\Delta f(x, y)$ is the shift in the precession frequency at point (x, y) in object space. If all of *k*-space were acquired at the same instant (at the same time *t*), off-resonance would not affect a reconstructed magnitude image. However, acquisition windows have durations on the order of 2 to 8 msec, which introduces off-resonance artifacts. Note that techniques that use longer readouts experience increased artifact.

One way to compensate for off-resonance is to acquire a field map to estimate $\Delta f(x, y)$ and to use this information to better reconstruct the final image. The field map or off-resonance map $\Delta f_m(x, y)$, can be computed by acquiring two images at different echo times and comparing the phase images at each location. These complex images would represent $M(x, y)e^{-2\pi i\Delta f(x,y)TE_1}$ and $M(x, y)e^{-2\pi i\Delta f(x,y)TE_2}$. The off-resonance term $\Delta f(x, y)$ is then simply found by computing the phase difference between these two images divided by the difference in echo times ($TE_2 - TE_1$).

METHOD

Pulse Sequence

Figure 1 illustrates the pulse sequence. Flow-compensated excitations are followed by radial spoke readouts and dephasing pulses in the slice-select direction. Every alternate spoke acquisition is delayed by a small amount labeled ΔTE. For convenience, delayed spokes are labeled ''late-TE'' spokes, and non-delayed ones are labeled ''early-TE'' spokes. Notice that this pulse sequence is identical to conventional PR except for the echo delay between early-TE and late-TE acquisitions.

Magnetic Resonance Systems Research Laboratory, Department of Electrical Engineering, Stanford University, Stanford, California.

Grant sponsors: National Institutes of Health; GE Medical Systems; Fannie and John Hertz Foundation.

*Correspondence to: Krishna S. Nayak, Packard 211, ISL, 350 Serra Mall, Stanford University, Stanford, CA 94305-9510. E-mail: nayak@lad.stanford.edu

Received 9 July 1999; revised 1 September 1999; accepted 13 September 1999.

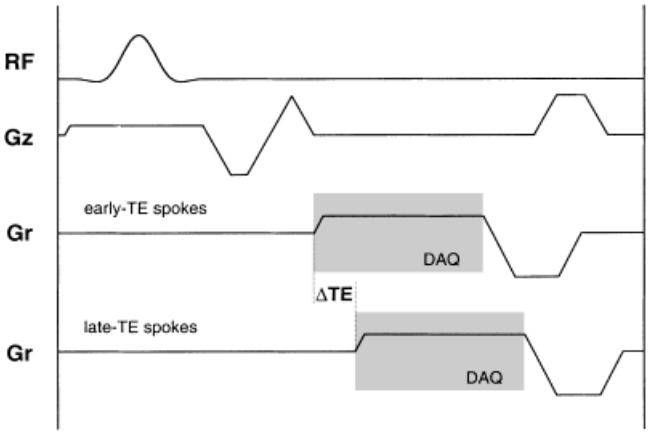

FIG. 1. Off-resonance corrected PR-pulse sequence: A small-tip excitation (flow-compensated excitation is shown) is followed by a refocused readout that acquires one radial spoke, and a crusher to dephase remaining signal. Late-TE acquisitions have a delayed readout and echo, as shown.

Field Map Computation

The central portion of *k*-space is then used to generate two lower resolution images with different echo times–one from the early-TE spokes and one from the late-TE spokes (see Fig. 2). These images are formed from *k*-space data within a disk of half the radius of the total extent covered in *k*-space. Each of these images are therefore of one-quarter resolution (i.e., half resolution in both the x and y directions). Since image FOV is related to the maximum spacing of *k*-space samples, both low-resolution images also have the same FOV as the final full-resolution image.

A field map $\Delta f_m(x, y)$ is then computed in a standard way, using the phase difference between the two low-resolution images, $I_{late\text{-}TE}$ and $I_{early\text{-}TE}$:

$$\Delta f_m(x, y) = \frac{\arg\left(I_{\text{late-TE}} I^*_{\text{early-TE}}\right)}{-2\pi\Delta\text{TE}} \qquad [3]$$

The measurable range of this field map (in Hz) is notably limited by the off-resonance that will cause a phase shift of $\pm\pi$ after ΔTE:

$$|\Delta f_m(x, y)| < \frac{1}{2\Delta\text{TE}} \qquad [4]$$

Since field map estimates are reliable in areas of sufficient signal, a smooth polynomial approximation $\Delta f_p(x, y)$ (12) is computed for use during reconstruction. This polynomial field map $\Delta f_p(x, y)$ is found using a weighted least-squares algorithm which minimizes:

$$\sum_{i,j} w_{ij}[\Delta f_p(x_i, y_j) - \Delta f_m(x_i, y_j)]^2 \qquad [5]$$

where w_{ij} measures the importance of minimizing the error at that voxel. The weighting used is proportional to the square magnitude of the voxel signal. In the final reconstruction step, we use this polynomial fit as our field map.

Image Reconstruction

Multifrequency image reconstruction is used to compensate for off-resonance in the image while simultaneously correcting for the different echo times (11,13). In multifrequency reconstruction, a finite set of frequency samples $\{f_n\}$ are selected such that they span the full range of off-resonance frequencies. For each f_n an image is reconstructed based on that frequency of precession. This is done by modulating the raw data of each readout by $e^{+2\pi i f_n t}$. In order to use both the early-TE and late-TE measurements for each f_n image, the sets are phase-aligned by multiplying the raw data from late-TE acquisitions by $e^{+2\pi i f_n \Delta TE}$. An image is then generated via gridding reconstruction (14) with both early-TE and late-TE data. For the final image, each voxel is estimated by interpolating between the images based on the closest $\{f_n\}$ frequency samples to $\Delta f(x, y)$.

In summary, early-TE and late-TE spokes are acquired at different echo times. A low-resolution field map is computed using the oversampled central region of *k*-space. Finally, multifrequency reconstruction is used to correct for off-resonance. This off-resonance correction is implemented with no additional scan time and a modest increase in reconstruction time.

RESULTS

Images shown here were acquired on a GE Signa 1.5 T system. PR acquisitions consisting of 512 radial spokes were used to achieve an image resolution of 163 × 163 pixels (0.98 mm resolution over a 16 cm circular FOV, or 0.74 mm resolution over a 12 cm circular FOV). Unless specified, each spoke readout lasted 8.192 ms, providing 256 samples. Off-resonance corrected PR images used a 1 msec ΔTE, 12th order polynomial fit (including cross terms) for the field map, and 10 frequency samples during

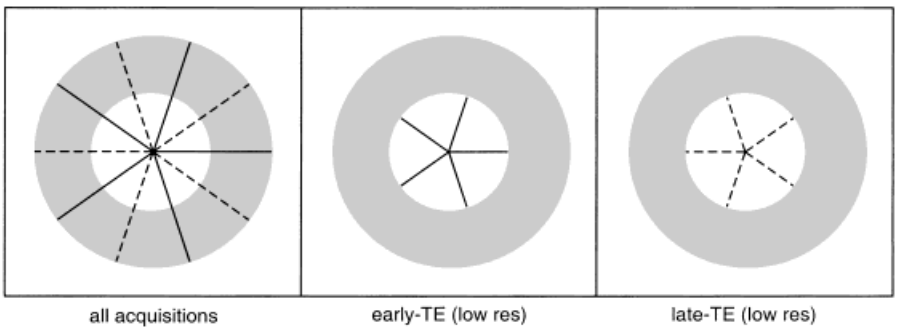

FIG. 2. *k*-space coverage. Of the full coverage (left), solid lines represent early-TE acquisitions and dotted lines represent late-TE acquisitions. Early-TE and late-TE low resolution images (middle and right) are each computed from half of the data in the central portion of *k*-space. These images have the same FOV as the final image, and have one-quarter the resolution—one-half in both x and y.

multifrequency reconstruction. A 1 msec ΔTE yields an off-resonance range of ±500 Hz.

Results of this technique applied to a resolution phantom are shown in Fig. 3. These images were acquired using a head coil, 16 cm FOV, 3 mm slice thickness, 300 msec TR, 4.5 msec TE, and 90° flip angle. Figure 3a is the result of a conventional PR scan (without ΔTE or off-resonance correction). Figure 3b–d show corresponding segments of the estimated field map, polynomial fit field map, and the corrected image using our new scan and reconstruction technique. The measured off-resonance was entirely within the range of [−38.3 to 19.4] Hz. The corrected image shows improved definition in the comb structure which is visible in cropped images (see Fig. 3e–f). This improvement is greater for sequences with long readouts, but is apparent even when imaging with shorter readouts.

To demonstrate this method in vivo, we applied it to peripheral angiography using 2D time of flight (TOF). Images were acquired using an extremity coil, 12 cm FOV, 3 mm slice thickness, 33 msec TR, 4.5 msec TE, and 60° flip angle. In this application, the presence of lipids and their chemical-shift causes sharp discontinuities in the acquired field map. To correct for smooth off-resonance variations

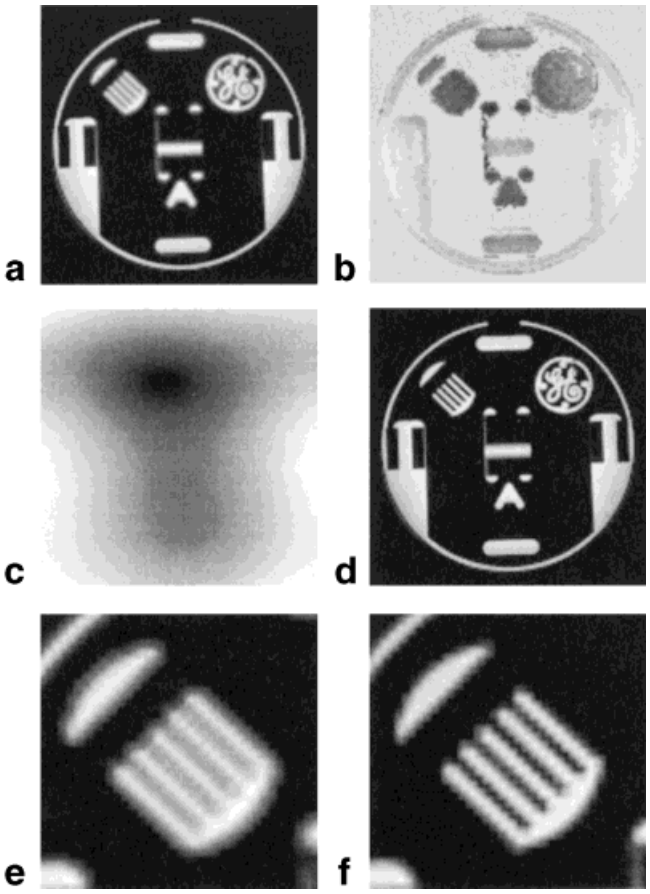

FIG. 3. Resolution phantom images using 8.192 msec readouts. Imaged with (**a**) conventional PR, and with off-resonance correcting PR resulting in images of the (**b**) acquired field map, (**c**) smooth polynomial fit field map, and (**d**) final reconstruction. The range of the field map images is −38.3 to 19.4 Hz. Close-ups of the comb structure in **a** and **d** are shown in **e** and **f.**

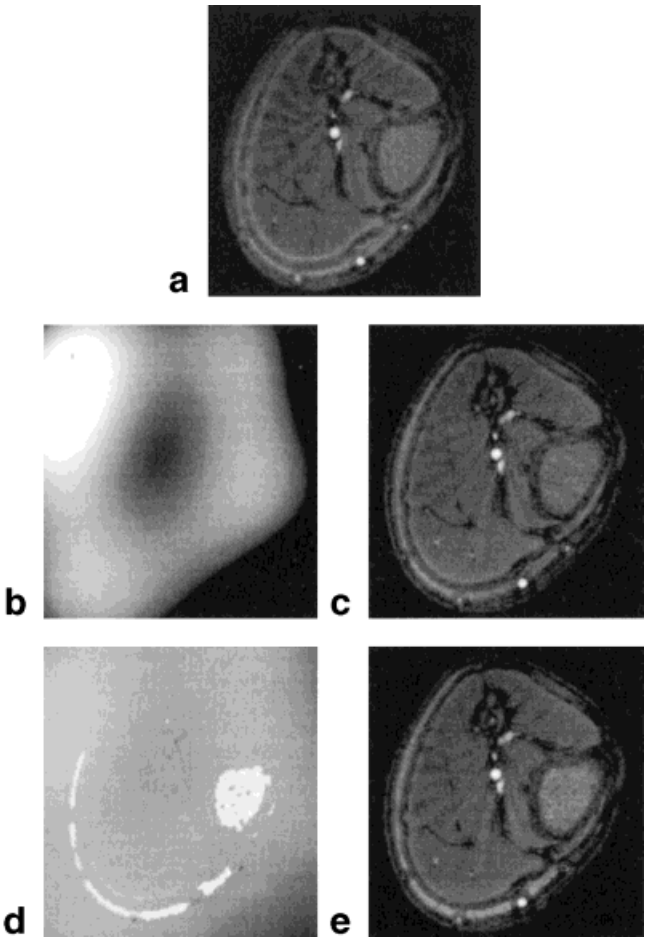

FIG. 4. In vivo example: An axial slice of the lower leg imaged with (**a**) conventional PR and (**b**–**e**) PR with off-resonance correction. For imaging vasculature, fat is ignored during field map approximation Δf_p (**b**) and the resulting corrected image (**c**) shows improved vessel definition. Alternatively, the computed field map Δf_m (**d**) can be used directly during reconstruction, resulting in (**e**) improved definition in areas of fat with added edge enhancement due to field map discontinuity.

(main field inhomogeneity), lipid voxels are excluded from the polynomial fitting. These lipid voxels are excluded by masking voxels with a measured Δf_m of at least 110 Hz below the center frequency of water. Figure 4 illustrates a conventional PR slice and the equivalent slice using our new acquisition and reconstruction scheme. When reconstructing these datasets, the field map estimate can be customized to the application. When using a polynomial fitted field map, with fat excluded from the fitting, slice images show improved vessel definition (see Fig. 4b–c). When using a hybrid field map consisting of the measured off-resonance in areas of high signal, and the smooth estimate elsewhere, resulting slice images show improved definition in vessels and areas of fat, while introducing some edge enhancement due to field map discontinuity (see Fig. 4d–e).

Figure 5 illustrates targeted maximum intensity projections (MIPs) of peripheral vasculature imaged with and without our technique. These images were acquired using an echo time of 6.3 msec, which places water and fat out-of-phase, and using a saturation pulse to suppress

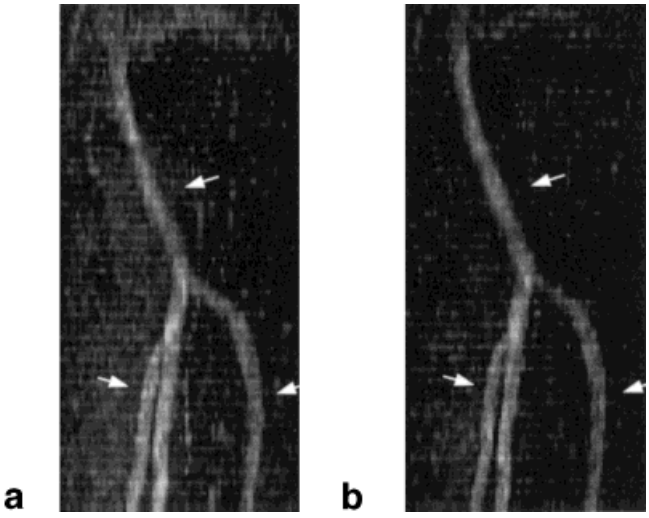

FIG. 5. Targeted maximum intensity projections of the popliteal trifurcation using multislice 2D TOF and venous saturation. Imaged using (**a**) conventional PR and (**b**) the presented off-resonance correcting PR. Notice the improved vessel definition and deblurring in areas of off-resonance, as indicated by arrows. Both images are windowed identically.

signal from veins. The MIPs constructed with off-resonance correction show improved vessel definition throughout the popliteal trifurcation and decreased blurring.

DISCUSSION

In summary, PR can be modified by interleaving delayed acquisitions with non-delayed acquisitions. This allows a low resolution field map to be computed with no additional scan time and only a slight increase in reconstruction time. Multifrequency reconstruction can then be used to compensate for off-resonance artifacts. Phantom and in vivo studies indicate this is a practical method for reducing off-resonance induced blurring. This technique is demonstrated with radial spoke acquisitions, but works for full projections as well.

This technique is a general one that is applicable to many different *k*-space trajectories that oversample the low spatial frequencies. It can be easily adapted for use with 3DPR, twisting radial lines (TwiRL), and variable density spiral (VDS) acquisitions. Ideal applications for this PR-based technique are applications that require short echo times, good flow and motion properties, and that suffer from off-resonance artifacts.

For imaging ultra short T_2 species, there is the added consideration of mixed contrast. Since images are formed from acquisitions at two echo times, differences in contrast between those two echoes will produce streaking artifacts. This streaking is similar to what is seen in angularly undersampled PR because both echo images are angularly undersampled during the final image reconstruction. In general, this off-resonance correcting technique is intended for areas where a small ΔTE does not significantly alter image contrast.

ACKNOWLEDGMENTS

This work was supported by the National Institutes of Health, GE Medical Systems, and by a Fannie and John Hertz Foundation Graduate Fellowship to Krishna S. Nayak. The authors thank Gerard Luk-Pat, Brian Hargreaves, Hatsumi Nielsen, and John Pauly for useful explanations and assistance.

REFERENCES

1. Gold GE, Pauly JM, Macovski A, Herfkens R. MR spectroscopic imaging of collagen: tendons and knee menisci. Magn Reson Med 1995;34:647–654.
2. Rasche V, de Boer RW, Holz D, Proksa R. Continuous radial data acquisition for dynamic MRI. Magn Reson Med 1995;34:754–761.
3. Glover G, Pauly J. Projection reconstruction techniques for reduction of motion effects in MRI. Magn Reson Med 1992;28:275–89.
4. Nishimura DG, Jackson JI, Pauly JM. On the nature and reduction of the displacement artifact in flow images. Magn Reson Med 1991;22:481–492.
5. Glover G, Lee A. Motion artifacts in fMRI: comparison of 2DFT with PR and spiral scan methods. Magn Reson Med 1995;33:624–35.
6. Smith PR, Peters TM, Bates RH. Image reconstruction from finite numbers of projections. J Phys A: Math, Nucl Gen 1973;6:361–383.
7. Scheffler K, Hennig J. Reduced circular field-of-view imaging. Magn Reson Med 1998;40:474–480.
8. Rasche V, Holz D, Kohler J, Roschmann P. Catheter tracking using continuous radial MRI. Magn Reson Med 1997;37:963.
9. Peters DC, Mistretta CA, Korosec FR, Holden J, Kelcz F, Wedding KL, Grist TM. Using projection reconstruction with a limited number of projections to increase image resolution or acquisition speed, In: Proceedings of the ISMRM 6th Annual Meeting, Sydney, Australia, 1998. p 182.
10. Noll DC, Pauly JM, Meyer CH, Nishimura DG, Macovski A. Deblurring for non-2d fourier transform magnetic resonance imaging. Magn Reson Med 1992;25:319–333.
11. Noll DC, Meyer CH, Pauly JM, Nishimura DG, Macovski A. A homogeneity correction method for magnetic resonance imaging with time-varying gradients. IEEE Trans Med Imag 1991;10:629–637.
12. Irarrazabal P, Meyer CH, Nishimura DG, Macovski A. Inhomogeneity correction using an estimated linear field map. Magn Reson Med 1996;35:278–282.
13. Nielsen HTC, Nishimura DG. Improved 2-D time-of-flight angiography using a radial-line *k*-space acquisition. Magn Reson Med 1997;37:285–291.
14. Jackson JI, Meyer CH, Dwight AM, Nishimura G. Selection of a convolution function for fourier inversion using gridding. IEEE Trans Med Imaging 1991;10:473–478 (September).